JOURNAL OF CHEMICAL INFORMATION AND MODELING

ARTICLE

pubs.acs.org/jcim

Computational Studies of Bacterial Resistance to β-Lactam Antibiotics: Mechanism of Covalent Inhibition of the Penicillin-Binding Protein 2a (PBP2a)

Nguyen Hoa My,[†] Hajime Hirao,[*,‡,§] Dang Ung Van,[†,⊥] and Keiji Morokuma[*,‡,∥]

[†]Faculty of Chemistry, Hanoi University of Natural Science, VNU, 19 Le Thanh Tong, Hanoi, Vietnam

[‡]Fukui Institute for Fundamental Chemistry, Kyoto University, 34-4 Takano Nishihiraki-cho, Sakyo, Kyoto 606-8103, Japan

[§]Division of Chemistry and Biological Chemistry, School of Physical and Mathematical Sciences, Nanyang Technological University, 21 Nanyang Link, Singapore 637371

[∥]Cherry L. Emerson Center for Scientific Computation and Department of Chemistry, Emory University, Atlanta, Georgia 30322, United States

[⊥]Hoa Binh University, CC2, My Dinh II, Tu Liem, Hanoi, Vietnam

Supporting Information

ABSTRACT: β-Lactam resistance of methicillin-resistant *Staphylococcus aureus* (MRSA), a pathogenic bacterium that causes staph infections, represents a serious threat to public health. This arises primarily due to the inability of β-lactam antibiotics to inhibit the transpeptidase activity of penicillin-binding protein 2a (PBP2a). Effective inhibition of PBP2a to prevent the bacterial cell wall biosynthesis is of great importance for the treatment of a variety of clinically challenging infectious diseases caused by MRSA. To gain fundamental insights into the mode of covalent inhibition of the enzyme, we have carried out computational studies of the acylation reactions between small β-lactam molecules (methicilin and nitrocefin) and PBP2a using the B3LYP/6-31G* and ONIOM(B3LYP/6-31G*:AMBER) hybrid quantum mechanical/molecular mechanical methods. Our calculations show that the acylation involves two transition states and that methicilin and nitrocefin undergo acylation in slightly different manners. The acylation of nitrocefin is more facile, which is attributed to the larger release of ring strain and the larger resonance stabilization gained upon ring opening. We suggest that, in addition to the nonbonded interactions between the ligand and the protein, these quantum chemical factors, which are associated with efficiency of the acylation step, should be taken into account and carefully controlled in designing novel β-lactam inhibitors of PBP2a.

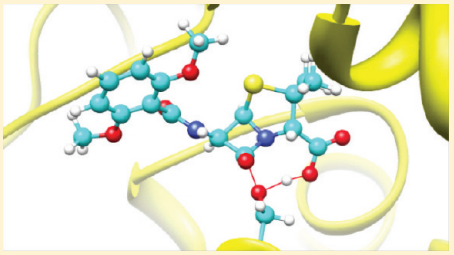

1. INTRODUCTION

Staphylococcus aureus (SA) is a pathogenic bacterium that is a common cause of staph infections. Longitudinal studies show that around 50% of human beings are nasal SA carriers, and the carriage of SA is associated with an increased risk of SA infection.[1,2] Symptoms of SA infections include ulcers, pustules, boils, and pneumonia, and surgical-site SA infection is another serious issue in hospitals. It used to be commonly believed that staph infections could be cured by penicillin antibiotics; however, in the early 1960s, emergence of a new β-lactam resistant strain of SA, called methicillin-resistant SA (MRSA), was reported.[2] This new strain acquired the mecA gene from an unidentified extra-species source, and the newly acquired mecA gene in MRSA encodes the protein penicillin-binding protein 2a (PBP2a)[4−13] that has transpeptidase activity. Because PBP2a shows only low affinity for β-lactams, it retains the capability to mediate cell wall cross-linking of MRSA, even in the presence of β-lactam antibiotics.

Inhibition of the PBP2a activity by a small molecule, which could result in cell lysis of the bacteria, should be regarded as the most direct approach to the treatment of MRSA infections. Conventional β-lactams, such as methicillin, do not inhibit the transpeptidase activity of PBP2a effectively. Therefore, alternative compounds should be designed in a manner that enables their stronger binding to the enzyme's active site. To do this in a rational way, it is imperative that the detailed molecular mechanism of β-lactam binding to PBP2a be understood. It is known that this binding process involves acylation, in which the hydroxyl group of Ser403 in the active site (Scheme 1) attacks the carbonyl carbon of the ligand. This acylation step leads to covalent bond formation of a β-lactam compound with Ser403.[14,15] As a result, the C−N bond of the β-lactam part is cleaved, while the carboxyl group forms a covalent bond with the serine hydroxyl group. The broad-spectrum resistance of MRSA to antibiotics should be associated with the reduction of the rate for the acylation reaction in PBP2a. Hence, the design of novel antibiotics will require

Received: September 6, 2011
Published: November 30, 2011

careful control of the energy barrier required for the acylation step.

Despite rough knowledge currently available for the acylation reactions in the active sites of PBPs, its detailed mechanism, especially in PBP2a, has yet to be elucidated. Conventional docking simulations may not be used to investigate such bond forming and breaking events, and quantum chemistry should be a more appropriate choice. In this work, we theoretically investigated the reactions between methicilin (MC1) and nitrocefin (NC1) (Scheme 2) and PBP2a using density functional theory (DFT) and hybrid QM/MM ONIOM(DFT:MM) approaches. In the MC1 and NC1 ligands, the β-lactam part is fused to thiazolidine and dihydrothiazine, respectively.

2. COMPUTATIONAL METHOD

2.1. Active-Site Models. To understand the intrinsic acylation reaction mechanism in the situation without the protein environment, we first performed quantum mechanical (QM) calculations on a simple active-site model. The model contained MC1 or NC1 (Scheme 2) plus CH_3OH that is a model of Ser403. These ligands have different substituents around the bicyclic part, namely L1 and R1 in MC1 and L2 and R2 in NC1 (Scheme 3). To evaluate the effect of the fundamental bicyclic structure of ligands on the reactivity, we also considered MC1′ and NC1′ that are devoid of substituents (Scheme 3).

QM calculations were performed at the B3LYP/6-31G* level. To characterize the potential energy surface of the reaction, relaxed scan calculations were performed by fixing a certain bond distance that can be assumed as a reaction coordinate while fully optimizing all the other coordinates. Subsequently, full geometry optimizations were performed for intermediates or transition states. No zero-point energy calculation was carried out.

2.2. Protein Models. A crystal structure of PBP2a (PDB code 1MWU) was used as a starting point of our study.[13] Only chain A of the enzyme was adopted. Figure 1 shows the active-site structure of the acylation complex between MC1 ligand and PBP2a, which corresponds to the product of the reaction in Scheme 1. In the PDB file, Ser403 and the MC1 ligand were defined as a single residue with a residue number 403. This was split into two separate residues.

Unfortunately, coordinates of a few residues were missing in the 1MWU file. The coordinates of Lys506, Lys604, Gly611, and Arg612 were therefore taken from another X-ray structure (PDB code 1VQQ) for the same protein in the apo form. The MOLDELLER software was used to add other missing residues (Met605, Lys606, Gln607, Gly608, Glu609, and Thr610).[16]

Scheme 1. Acylation Mechanism in Which the β-Lactam Carbonyl Is Attacked by a Serine Residue in the Active Site

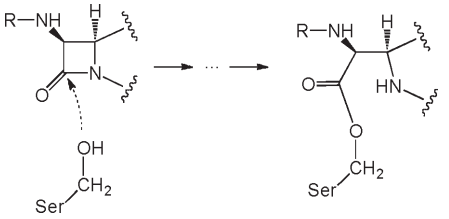

Scheme 3. Ligand Models for QM Calculations

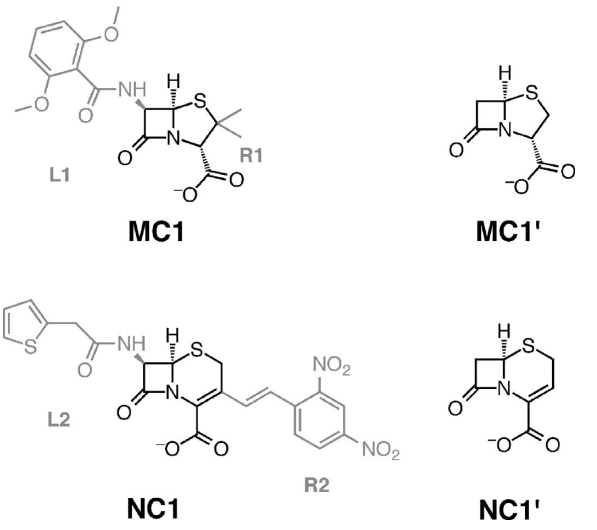

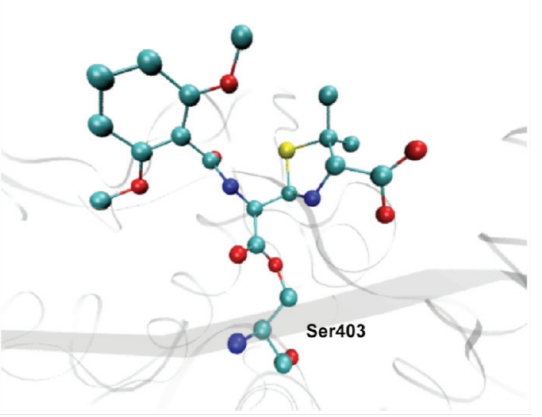

Figure 1. X-ray structure of PBP2a in complex with MC1 (PDB code 1MWU).[13]

Scheme 2. MC1 and NC1 Ligands

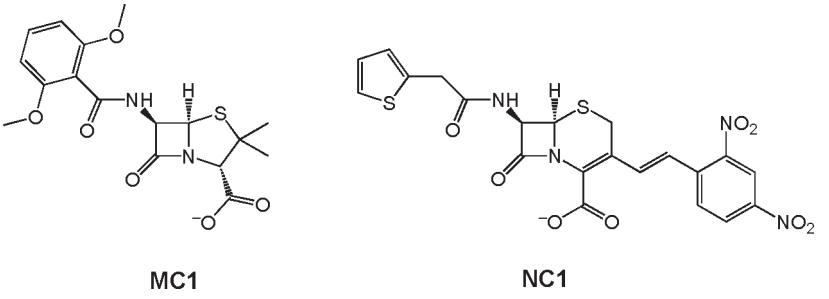

dx.doi.org/10.1021/ci2004175 |J. Chem. Inf. Model. 2011, 51, 3226–3234

Subsequently, hydrogen atoms were added with VMD software.[17] We performed PROPKA analysis[18,19] and visual inspection of 1MWU.pdb to determine the protonation states of His129 and His293 as HIE and the other His residues as HID. Here, HID and HIE follow the AMBER nomenclature system and stand for neutral histidines with protonated $N_{\delta 1}$ and $N_{\varepsilon 2}$ atoms, respectively. The atomic charges of the ligands were determined by the restrained electrostatic potential (RESP) method using Gaussian 09[20] and ANTECHAMBER.[21] In doing this, we optimized the geometries of the ligands at the B3LYP/6-31G* level.[22−25]

At first we performed geometry optimization of the entire enzyme by the AMBER molecular mechanical (MM) method[26] implemented in Gaussian 09 to obtain a good initial geometry for the subsequent ONIOM calculations. Since complete MM parameters are not available for the MC1 ligand, the atoms in the QM region (see below) were fixed throughout the MM calculations. It should be noted that in subsequent ONIOM calculations (next paragraph), the ligand was treated by a QM method and optimized. The ligand geometry in the PDB file corresponds to an acylation product. Therefore, we slightly modified the geometry of the ligand to prepare the geometry for a preacylation Michaelis complex, namely, the state before reaction. More specifically, the broken four-membered ring in the X-ray structure was closed to make an MC1 model. MM calculations were performed in a stepwise manner as follows. First, we optimized only hydrogen atoms in the system, while fixing the rest of the atoms. An atomic charge of −0.055 was given to the H-link atom of Ser403, so that the total AMBER charge of the serine QM atoms is zero. The system contained as many as 642 residues (10 483 atoms). Therefore, we searched for all residues in 1MWU.pdb that have at least one atom within 20 Å from the hydroxyl oxygen of Ser403. These residues were allowed to move in subsequent geometry optimizations, while all atoms outside of this region were kept fixed. In the first step, the backbone atoms in the optimized region were constrained, and only the side chains of residues were optimized. The constraints imposed on the backbone atoms were then released; thus, all atoms in the 20 Å radius were optimized. Still, QM atoms were frozen at this stage.

We then performed geometry optimizations for the region defined by the 20 Å radius (see above) with the ONIOM-(B3LYP/6-31G:AMBER) and then the ONIOM(B3LYP/6-31G*:AMBER) method.[27−30] The mechanical embedding scheme of ONIOM (ONIOM-ME) was used for geometry optimization, and the electronic embedding scheme (ONIOM-EE) was also used for single-point calculations. The ligand and the side chain of Ser403 were treated quantum mechanically. As for the MC1 reaction, the first step of the reaction was assumed to be the attack of the serine OH group on the carbonyl group in the β-lactam of the ligand. Therefore we used the C−O distance as the reaction coordinate. Relaxed scan calculations were performed by gradually changing the C−O distance while fully optimizing all the other coordinates (the QM and MM parts within 20 Å). The second step of the reaction was assumed to be cleavage of the N−C bond of β-lactam. Therefore relaxed scan calculations here were performed using the N−C distance as the reaction coordinate.

In order to make a fair comparison between the reactions of MC1 and NC1, the ONIOM-optimized geometry of the MC1 complex was used as the starting point for the calculations of the NC1 complex. The coordinates of MC1 were replaced by those of NC1 taken from an X-ray structure (PDB code 1MWS). Since the PDB file for the NC1 complex was for an acylation complex (after reaction), we prepared coordinates for a preacylation complex manually adjusting the geometry, as we did for the MC1 complex. In the relaxed scan, the C−O bond distance was also used as the reaction coordinate for the first step of the NC1 reaction. However, it was found that the N−C bond was easily broken in the first step of the NC1 reaction, and the second step was proton transfer from the oxygen atom of the carboxyl group to the nitrogen atom. Therefore, we used the N−H distance as the reaction coordinate for the second step of the NC1 reaction.

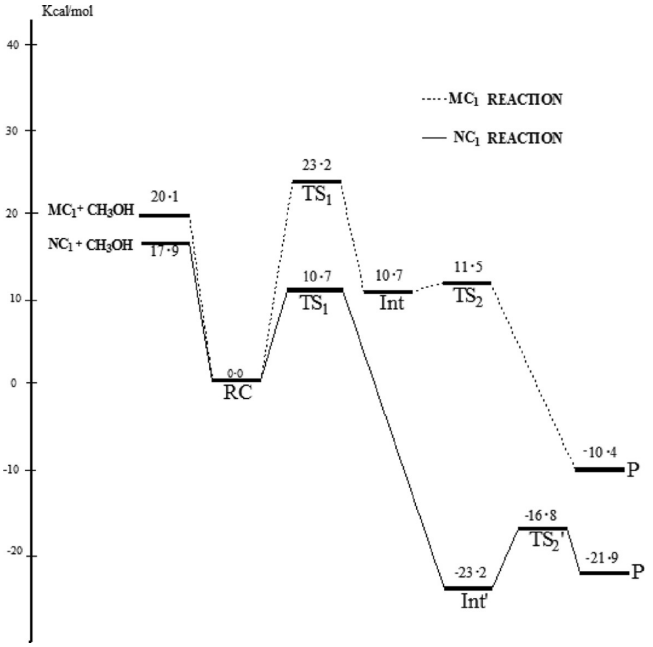

Figure 2. Energy profiles (in kcal/mol) obtained for the active site QM models.

Table 1. Relative Energies (in kcal/mol) of Reactant Complex, Transition States, Intermediates, and Products of the MC1 and NC1 Reactions

	RC	TS1	Int (Int′)	TS2 (TS2′)	P
QM					
MC1	0.0	23.2	10.7	11.5	−10.4
MC1′	0.0	22.2	−12.6	3.9	−8.8
NC1	0.0	10.7	−23.2	−16.8	−21.9
NC1′	0.0	16.6	−6.1	−12.9	−12.9
ONIOM-ME					
MC1	0.0	33.0	17.0	18.9	−18.1
NC1	0.0	21.3	−26.6	−23.1	−31.0
ONIOM-EE					
MC1	0.0	37.1	23.6	23.5	−6.2
NC1	0.0	26.8	−3.5	−4.5	−16.6

3. RESULTS AND DISCUSSION

3.1. Energy Profiles for Active Site Models. The energy profiles for the active site QM models are shown in Figure 2

dx.doi.org/10.1021/ci2004175 |J. Chem. Inf. Model. 2011, 51, 3226–3234

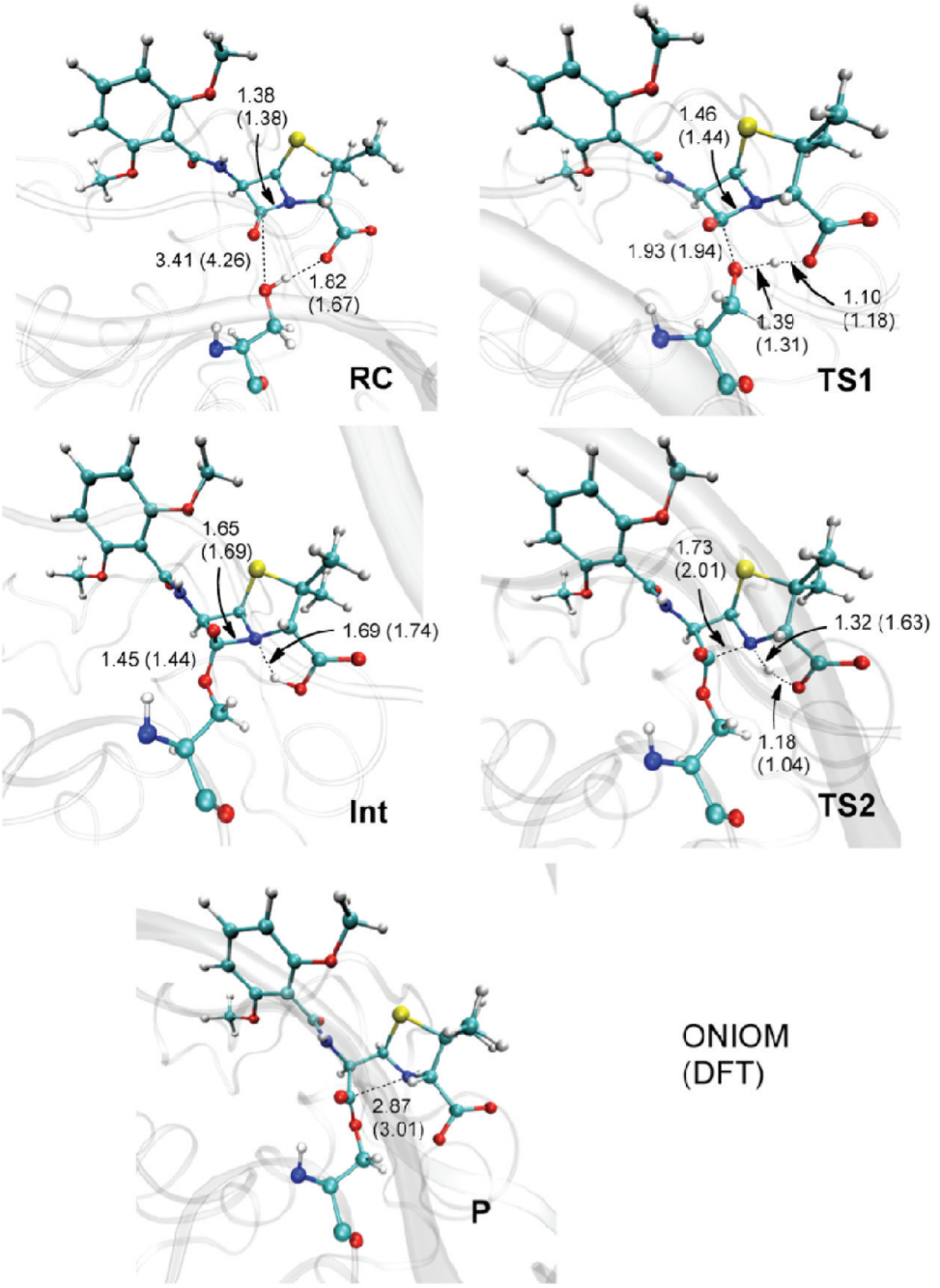

Figure 3. Optimized geometries (bond distances in Å) for the MC1 reaction for the enzyme ONIOM(DFT:MM) and active-site QM models (in parentheses).

(see also Table 1). The energy barrier for the C−O bond formation reaction for MC1 reaction is higher than that for NC1 by 12.5 kcal/mol. This result is consistent with the experimental result that NC1 has a higher acylation rate than MC1.[12] Calculations show that the MC1 reaction proceeds in a stepwise manner. In the first step of the reaction, a C−O bond is formed, and in the second step, N−C bond cleavage takes place. Figures 3 and 4 show the optimized geometries for the intermediates and transition states of the MC1 and NC1 reactions, respectively. For MC1, in the reactant complex (**RC**), the long distance between the serine hydroxyl oxygen and the carbonyl carbon of the ligand, 4.26 Å, is shortened to 1.94 and 1.44 Å at the transition state (**TS1**) and intermediate (**Int**), respectively. In the first C−O bond formation step of the MC1 reaction (**RC** to **Int**), the proton of the OH group of Ser403 (modeled by methanol) was transferred to the carboxylate oxygen of the ligand, and at the same time a bond was formed between the serine oxygen and carbonyl carbon atoms. Thus, the carboxyl group of the ligand is acting as a catalytic base that promotes deprotonation of Ser403 and enhances its reactivity. This is markedly different from the likely mechanism in β-lactamases, for which the nearby Glu166 or Lys73 was proposed to act as a catalytic base.[31−35] Because the active-site model calculation does not take into account the presence of surrounding amino acid residues, the use of a full

dx.doi.org/10.1021/ci2004175 |*J. Chem. Inf. Model.* 2011, 51, 3226–3234

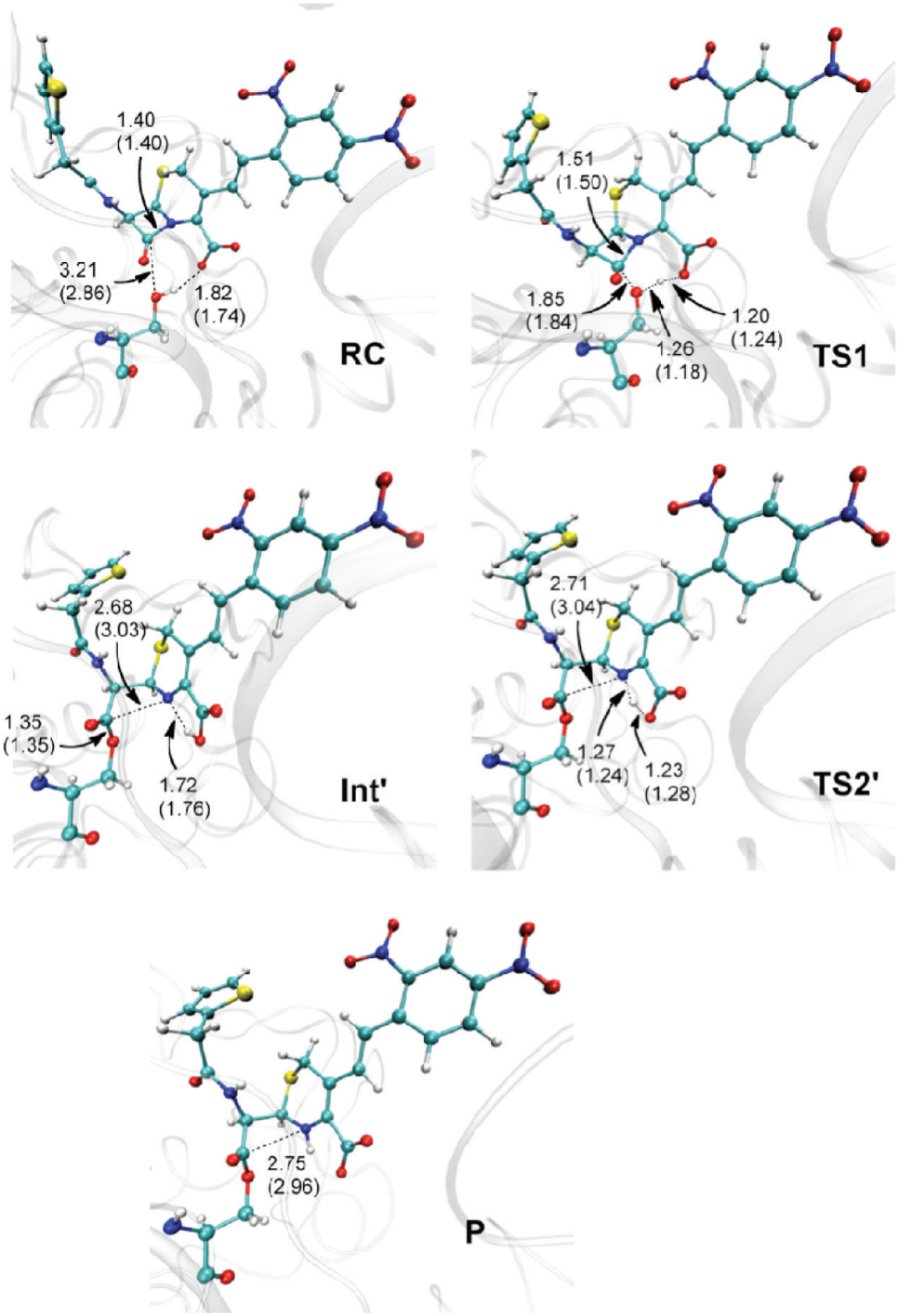

Figure 4. Optimized geometries (bond distances in Å) for the NC1 reaction for the enzyme ONIOM(DFT:MM) and active-site QM models (in parentheses) .

protein model might provide different results. However, as we shall see later, the Ser403 has a favorable H-bond with the carboxylate of the MC1 ligand in the ONIOM-optimized geometry of **RC**. Furthermore, there is no Asp or Glu residue to which a proton of Ser, water, or Lys could be transferred. Therefore, it seems likely that the carboxylate group of the ligand acts as a catalytic base in the reactions of PBP2a. At the transition state **TS1**, the proton transfer from Ser403 to the carboxylate group is significantly advanced, increasing the nucleophilicity of the serine hydroxy group to promote the C−O bond formation. In the next step, the N−C bond of the four-membered ring of MC1 in **Int** is cleaved via **TS2** to yield the final acylation product (**P**). The ligand conformation in **P** was essentially the same as that in the crystal structure, but the orientations of the carboxyl group on the thiazolidine ring in these two structures were slightly different (Figure S2, Supporting Information). In the computed structure, the carboxyl group formed a salt-bridge interaction with Lys597, whereas in the crystal structure, this interaction was not

dx.doi.org/10.1021/ci2004175 |*J. Chem. Inf. Model.* 2011, 51, 3226–3234

Table 2. Electrostatic and vdW Interaction Energies between the QM Atoms and the Protein Environment (in kcal/mol)

	RC	TS1
	MC1	
E_{es}	−173.2	−166.3
E_{vdW}	−47.2	−47.3
	NC1	
E_{es}	−127.6	−121.0
E_{vdW}	−47.6	−49.3

observed. The slightly different orientations of the carboxyl group are attributed to the somewhat different conformations of Lys597. These might indicate that there is additional reorientation of Lys597 after formation of **P**.

The mechanism of the NC1 reaction is similar to that of MC1 in some respects but different in others. The structure of **TS1** for the NC1 reaction with the O(Ser403)···H(Ser403), H(Ser403)···O(carboxylate), and O(Ser403)···C(carbonyl) distances of 1.18, 1.24, and 1.84 Å, respectively, is qualitatively similar to that of **TS1** for the MC1 reaction with the corresponding distances of 1.31, 1.18, and 1.94 Å, respectively. However, closer inspection reveals that the migrating proton remains close to Ser403 at **TS1** for the NC1 reaction, as obtained with the active site model, compared with **TS1** for the MC1 reaction in which the proton transfer to the carboxylate is more advanced. On the other hand, the O(Ser403)···C(carbonyl) distance in NC1 is a little shorter than in MC1 at **TS1**, suggesting that this O−C bond formation is more advanced in **TS1** of the NC1 reaction. After **TS1**, the N−C bond in the four-membered ring was easily broken in the NC1 reaction. At the stage of the subsequent intermediate (**Int′**), the N−C bond was completely cleaved. This intermediate is different from the N−C cleaved product of the MC1 reaction (**P**), in that the proton from Ser403 is bound to the carboxylate in the former and to the nitrogen atom in the latter. The proton is then transferred in the second step via **TS2′** to the nitrogen atom to form a final product (**P**) in the NC1 reaction. A prime was used in **Int′** and **TS2′** to indicate that their nature is different from that of the corresponding species in the MC1 reaction. In the MC1 reaction, the N−C bond has not been broken at **Int** and **TS2** involves concomitant N−C bond cleavage and proton transfer (Figure 3). By contrast, the N−C bond is already broken at **Int′** in the NC1 reaction, and the **TS2′** is characterized solely as proton transfer from the carboxylate to nitrogen (Figure 4).

3.2. Energy Profiles for Protein Models. Figures 3 and 4 also show the ONIOM-calculated geometric parameters for the protein models. It can be seen that in the protein environment, the reaction mechanisms for the two reactions were essentially the same as those obtained using the active site models. However, the energy barriers for the first step were calculated to be higher at the ONIOM-ME level in the protein environment than those for the active-site models by ∼10 kcal/mol (Table 1). The barrier calculated with ONIOM-EE was even higher, 37.1 and 26.8 kcal/mol for the MC1 and NC1 reactions, respectively. The high barrier obtained for MC1 is consistent with the poor inhibitory activity of methicillin toward PBP2a. Furthermore, the relatively high barrier obtained for the NC1 reaction indicates that there is still room for improvement regarding the inhibitory activity of β-lactam compounds. As pointed out previously, the distorted

Scheme 4. Key Residues around the Ligands at TS1

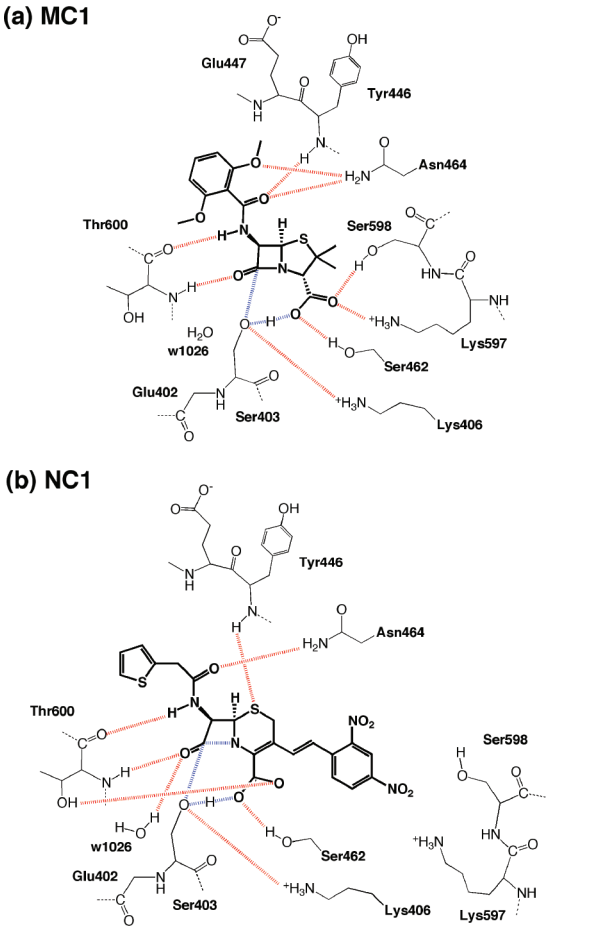

active site of the enzyme, especially a strand β3 and helix α2, should also be another important factor that causes less efficient binding of β-lactams to the active site.[13]

Careful analyses of the electrostatic and van der Waals (vdW) interactions between the QM atoms (excluding the H-link atom) and the surrounding residues revealed that the steric effect, as estimated from vdW interaction energies for **RC** and **TS1**, is not necessarily unfavorable for the C−O bond formation step. Rather, the increase in the barrier height in the protein environment is largely due to the less favorable electrostatic interaction at **TS1**. Table 2 summarizes electrostatic (E_{es}) and vdW (E_{vdW}) interaction energies for **RC** and **TS1** of the two reactions. Interactions between the ligands and nearby residues at **TS1** are schematically illustrated in Scheme 4. The electrostatic stabilization of the active site is more than 6 kcal/mol smaller at **TS1** than at **RC**, whereas the vdW interaction is slightly more favorable at **TS1**. The major contributors to this electrostatic destabilization are: w1026 (+9.5 kcal/mol), Ser462 (+2.6 kcal/mol), Ser403 (+2.5 kcal/mol), Ser598 (+2.0 kcal/mol), Gly402 (+1.5 kcal/mol), and Glu447 (+1.3 kcal/mol) for the MC1 reaction, and Ser462 (+3.6 kcal/mol), Thr600 (+3.0 kcal/mol), Lys406 (+1.7 kcal/mol), Asn464 (+1.4 kcal/mol), and w1026 (+1.3 kcal/mol) for the NC1 reaction. The water molecule (w1026) has a H-bond interaction with the carbonyl oxygen of MC1 and with the hydroxyl oxygen of Ser403 in **RC**. However, these H-bonds are disrupted at **TS1**, resulting in large electrostatic destabilization.

In contrast, w1026 has a H-bond only with the carbonyl oxygen in **RC** of the NC1 reaction, and this H-bond is retained at **TS1**. Therefore, electrostatic destabilization due to w1026 is less severe in the NC1 reaction. Destabilizations caused by other residues are due to less efficient H-bond interactions at **TS1**. To improve the inhibitory activity of these β-lactam compounds, these electrostatic destabilization effects should be mitigated. A few residues are found to stabilize the transition states. In the MC1 reaction, the effects of Lys406 (−4.1 kcal/mol), Thr600 (−2.3 kcal/mol), and Tyr446 (−1.8 kcal/mol) are relatively large, whereas in the NC1 reaction, the effect of Lys597 (−3.3 kcal/mol) is relatively large. Lys406 forms a H-bond with the hydroxyl group of Ser403. It should also be noted that the H-bond interaction of Lys406 with Ser403 will lower the reactivity of the deprotonated Ser403. This should be why the ONIOM-EE produced higher barriers than DFT and ONIOM-ME.

Compared to the barriers obtained for the active-site models, the energy barriers for the second steps for both MC1 and NC1 reactions were low, 1.9 and 3.5 kcal/mol, respectively, in ONIOM-ME calculations, and the barriers disappeared in ONIOM-EE calculations. All calculations, therefore, suggest that the first step (C−O bond formation) should be the rate-limiting step.

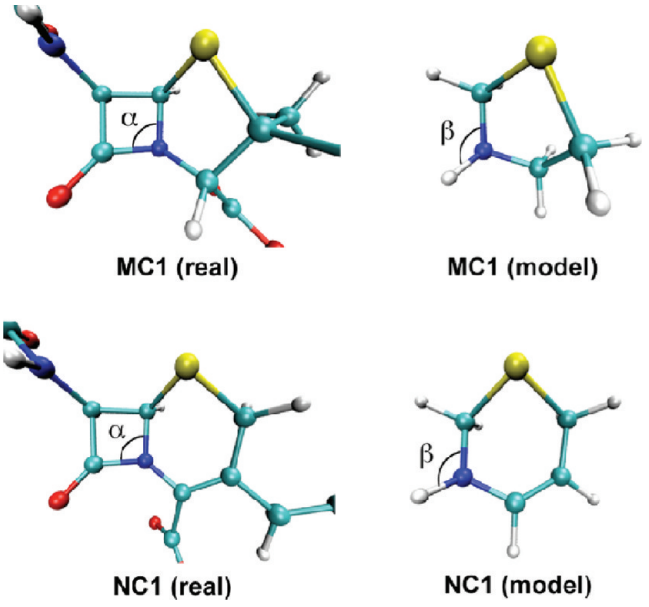

Figure 5. Definitions of strain angles for MC1 and NC1 ligands and simplified versions.

Table 3. Strain Angles for the Ligands (in degrees), as Defined in Figure 5

	α	β	$\lvert\alpha - \beta\rvert$
MC1	94.2	109.1	14.9
NC1	95.1	114.3	19.2

3.3. Reason for the Difference in Reactivity Between MC1 and NC1. The above analyses showed that the β-lactam N−C bond is cleaved more easily in NC1. This may be attributed to the difference in strain energy of the four-membered rings in MC1 and NC1. To examine this hypothesis, we carried out further analyses using the MC1 and NC1 ligands and simplified ligands, namely, thiazolidine and dihydrothiazine, respectively (Figure 5). The actual ligands have four-membered rings that should have large strain energies because of the small C−N−C angles (α). The simplified molecules, however, do not possess a β-lactam four-membered ring and thus do not store strain energy. In the simplified ligands, the carbon atoms attached to the five- or six-membered rings are replaced with hydrogen atoms, and the strain angle is defined as β, corresponding to α of the parent molecules. The relative strain (or the release of strain) of β-lactam may be estimated from $|\alpha - \beta|$. Table 3 summarizes the strain angles for the actual and simplified ligands. The α values for MC1 (94.2°) and NC1 (95.1°) are similar, because of the tight four-membered arrangement of atoms. However, the β values for the simplified ligands are seen to be different: 109.1° for MC1 and 114.3° for NC1. Mainly because of the large difference in the β values, the $|\alpha - \beta|$ value of NC1 is larger than that for MC1 by 4.3°. This indicates that NC1 stores larger strain energy in the β-lactam part, and a larger stabilization can be attained when the N−C bond is broken.

The reason why the intermediate (**Int′**) is very stable in the NC1 reaction may be due to a larger resonance stabilization (Scheme 5). The substituent attached to the six-membered dihydrothiazine ring allows the negative charge on the β-lactam nitrogen generated after the cleavage of the N−C bond to be substantially delocalized. In support of our hypothesis, **Int′** was much less stable in NC1′ than that of NC1, because it does not have the conjugated substituent on the six-membered ring (Table 1).

4. CONCLUSION

We have studied the acylation reactions of the MC1 and NC ligands with the PBP2a enzyme, using active-site and protein models. It was shown that the energy barrier for the NC1 reaction is lower than that for the MC1 reaction by about 10 kcal/mol. This is consistent with the enhanced rate of acylation of NC1, compared to the case of MC1. The mechanism of the acylation of NC1 is slightly different from that of MC1. The reaction between NC1 and PBP2a leads in the first step to an intermediate resembling the product. The second step is just associated with proton transfer from the caboxylate oxygen to the nitrogen atom in the four-membered ring. The barrier for the latter is much lower than that for the first step. Compared to the MC1 ligand, the ring strain is larger for the NC1 ligand, which appears to be the major reason for the enhanced rate of the NC1

Scheme 5. Resonance Stabilization in Int′ of NC1

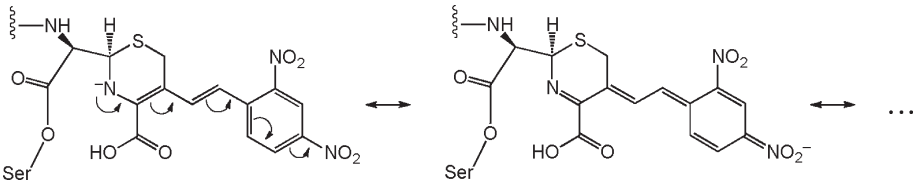

reaction. It is also likely that the resonance effect contributes to the higher reactivity of NC1.

Despite the higher reactivity of NC1, there remains room for improvement in that molecule. There seem to be two promising strategies that focus on the acylation step. The first strategy is to mitigate the electrostatic destabilization effect, which may be made possible by careful design of substituents. Second, the activation barrier for the acylation reaction between and β-lactams Ser403 should be lowered. In essence, key determinants of the barrier heights are the ring strain and the resonance effect. For the control and improvement of such aspects of drugs, quantum mechanical methods are more suitable than coventional docking protocols that rely on molecular mechanics.

■ ASSOCIATED CONTENT

Supporting Information. Full ref 20, assigned AMBER atom types for the QM atoms, comparison of MC1 ligand conformations in the crystal structure and the ONIOM-optimized product state, and XYZ coordinates of optimized structures. This information is available free of charge via the Internet at http://pubs.acs.org.

■ AUTHOR INFORMATION

Corresponding Author

*E-mail: hirao@ntu.edu.sg; morokuma@fukui.kyoto-u.ac.jp.

■ ACKNOWLEDGMENT

This work was in part supported by the Japan-East Asia Network of Exchange for Students and Youths (JENESYS) program of Japan Society for the Promotion of Science (JSPS) at the Fukui Institute for Fundamental Chemistry (FIFC). H.H. thanks the FIFC Fellowship and Nanyang Assistant Professorship for financial support and the High Performance Computing Centre (HPCC) at Nanyang Technological University for computer resources. This work was in part supported by a CREST grant in the Area of High Performance Computing for Multiscale and Multiphysics Phenomena from the Japan Science and Technology Agency (JST).

■ REFERENCES

(1) Wertheim, H. F. L.; Melles, D. C.; Vos, M. C.; van Leeuwen, W.; van Belkum, A.; Verbrugh, H. A.; Nouwen, J. L. The Role of Nasal Carriage in *Staphylococus aureus* Infections. *Lancet Infect. Dis.* **2005**, *5*, 751–762.

(2) Frank, D. N.; Feazel, L. M.; Bessesen, M. T.; Price, C. S.; Janoff, E. N.; Pace, N. R. The Human Nasal Microbiota and *Staphylococcus aureus* Carriage. *PLoS One* **2010**, *5*, e10598.

(3) Jevons, M. P. "Celbenin" - Resistant Staphylococci. *Br. Med. J.* **1961**, *1*, 124–125.

(4) Fisher, J. F.; Meroueh, S. O.; Mobashery, S. Bacterial Resistance to β-Lactam Antibiotics Compelling Opportunism, Compelling Opportunity. *Chem. Rev.* **2005**, *105*, 395–424.

(5) Guignard, B.; Entenza, J. M.; Moreillon, P. β-Lactams Against Methicillin-Resistant *Staphylococcus aureus*. *Curr. Opin. Microbiol.* **2005**, *5*, 479–489.

(6) Wilke, M. S.; Lovering, A. L.; Strynadka, N. C. J. β-Lactam Antibiotic Resistance: A Current Structural Perspective. *Curr. Opin. Microbiol.* **2005**, *8*, 525–533.

(7) Lu, W. P.; Sun, Y.; Bauer, M. D.; Paule, S.; Koenigs, P. M.; Kraft, W. G. Penicillin-Binding Protein 2a from Methicillin-Resistant *Staphylococcus aureus*: Kinetic Characterization of Its Interactions with β-Lactams Using Electrospray Mass Spectrometry. *Biochemistry* **1999**, *38*, 6537–6546.

(8) Crisostomo, M. I.; Westh, H.; Tomasz, A.; Chung, M.; Oliveira, D. C.; de Lencastre, H. The Evolution of Methicillin Resistance in *Staphylococcus aureus*: Similarity of Genetic Backgrounds in Historically Early Methicillin-Susceptible and Resistant Isolates and Contemporary Epidemic Clones. *Proc. Natl. Acad. Sci. U.S.A.* **2001**, *98*, 9865–9870.

(9) Pinho, M. G.; de Lencastre, H.; Tomasz, A. An Acquired and A Native Penicillin-Binding Protein Cooperate in Building the Cell Wall of Drug-Resistant Staphylococci. *Proc. Natl. Acad. Sci. U. S. A.* **2001**, *98*, 10886–10891.

(10) Hiramatsu, K.; Cui, L.; Kuroda, M.; Ito, T. The Emergence and Evolution of Methicillin-Resistant *Staphylococcus aureus*. *Trends Microbiol.* **2001**, *9*, 486–493.

(11) Fuda, C.; Suvorov, M.; Vakulenko, S. B.; Mobashery, S. The Basis for Resistance to β-Lactam Antibiotics by Penicillin-binding Protein 2a of Methicillin-resistant *Staphylococcus aureus*. *J. Biol. Chem.* **2004**, *279*, 40802–40806.

(12) Fuda, C.; Hesek, D.; Lee, M.; Heilmayer, W.; Novak, R.; Vakulenko, S. B.; Mobashery, S. Mechanistic Basis for the Action of New Cephalosporin Antibiotics Effective Against Methicillin- and Vancomycin-resistant *Staphylococcus aureus*. *J. Biol. Chem.* **2006**, *281*, 10035–10041.

(13) Lim, D.; Strynadka, N. C. J. Structural Basis for the β-Lactam Resistance of PBP2a from Methicillin-Resistant *Staphylococcus aureus*. *Nat. Struct. Biol.* **2002**, *9*, 870–876.

(14) Graves-Woodward, K.; Pratt, R. F. Reaction of Soluble Penicillin-Binding Protein 2a of Methicillin-Resistant *Staphylococcus aureus* with β-Lactams and Acyclic Substrates: Kinetics in Homogeneous Solution. *Biochem. J.* **1998**, *332*, 755–761.

(15) Zhao, G.; Meier, T. I.; Hoskins, J.; McAllister, K. A. Identification and Characterization of the Penicillin-Binding Protein 2a of *Streptococcus pneumoniae* and Its Possible Role in Resistance to β-Lactam Antibiotics. *Antimicrob. Agents Chemother.* **2000**, *44*, 1745–1748.

(16) Eswar, N., Webb, B., Marti-Renom, M. A., Madhusudhan, M. S., Eramian, D., Shen, M. Y., Pieper, U., Sali, A. *Current Protocols in Bioinformatics*; Wiley-Interscience: New York, 2006; Chapter 5, Unit 5.6.

(17) Humphrey, W.; Dalke, A.; Schulten, K. VMD - Visual Molecular Dynamics. *J. Mol. Graphics* **1996**, *14*, 33–38.

(18) Li, H.; Robertson, A. D.; Jensen, J. H. Very Fast Empirical Prediction and Rationalization of Protein pKa Values. *Proteins* **2005**, *61*, 704–721.

(19) Bas, D. C.; Rogers, D. M.; Jensen, J. H. Very Fast Prediction and Rationalization of pK_a Values for Protein−Ligand Complexes. *Proteins* **2008**, *73*, 765–783.

(20) Frisch, M. J.; Trucks, G. W.; Schlegel, H. B.; Scuseria, G. E.; Robb, M. A.; Cheeseman, J. R.; Montgomery, J. A., Jr.; Vreven, T.; Kudin, K.; Burant, J. C.; Millam, J. M.; Iyengay, S. S.; Tomasi, J.; Barone, V.; Mennucci, B.; Cossi, M.; Scalmani, G.; Rega, N.; Petersson, G. A.; Nakatsuji, H.; Hada, M.; Ehara, M.; Toyota, K.; Fukuda, R.; Hasegawa, J.; Ishida, M.; Nakajima, T.; Honda, Y.; Kitao, O.; Nakai, H.; Klene, M.; Li, X.; Knox, J. E.; Hratchian, H. P.; Cross, J. B.; Adamo, C.; Jaramillo, J.; Comperts, R.; Startmann, R. E.; Yazyev, O.; Austin, A. J.; Cammi, R.; Pomelli, C.; Ochterski, J. W.; Ayala, P. Y.; Morokuma, K.; Voth, G. A.; Salvador, P.; Dannenbuerg, J. J.; Zakrzewski, V. G.; Dapprich, S.; Daniels, A. D.; Strain, M. C.; Farkas, O.; Malick, D. K.; Rabuck, A. D.; Raghavachari, K.; Foresman, J. B.; Ortiz, J. V.; Cui, Q.; Baboul, A. G.; Clifford, S.; Cioslowski, J.; Stefanov, B. B.; Liu, G.; Liashenko, A.; Piskorz, P.; Komaromi, I.; Martin, R. L.; Fox, D. J.; Keith, T.; Al-Laham, M. A.; Peng, C. Y.; Nanayakkara, A.; Challacombe, M.; Gill, P. M. W.; Johnson, B.; Chem, W.; Wong, M. W., Gonzalez, C.; Pople, J. A. *Gaussian 09*, revision A.02; Gaussian, Inc: Wallingford, CT, 2009.

(21) Wang, J.; Wang, W.; Kollman, P. A.; Case, D. A. Automatic Atom Type and Bond Type Perception in Molecular Mechanical Calculations. *J. Mol. Graphics Modell.* **2006**, *25*, 247–260.

(22) Becke, A. D. Density-Functional Thermochemistry. III. The Role of Exact Exchange. *J. Chem. Phys.* **1993**, *98*, 5648–5652.

(23) Lee, C.; Yang, W.; Parr, R. G. Development of the Colle-Salvetti Correlation-Energy Formula into a Functional of the Electron Density. *Phys. Rev. B* **1988**, *37*, 785–789.

(24) Vosko, S. H.; Wilk, L.; Nusair, M. Accurate Spin-Dependent Electron Liquid Correlation Energies for Local Spin Density Calculations: a Critical Analysis. *Can. J. Phys.* **1980**, *58*, 1200–1211.

(25) Hehre, W.; Radom, L.; Schleyer, P v. R.; Pople, J. A. *Ab Initio Molecular Orbital Theory*; John Wiley & Sons: New York, 1986.

(26) Cornell, W. D.; Cieplak, P.; Bayly, C. I.; Gould, I. R.; Merz., K. M., Jr.; Ferguson, D. M.; Spellmeyer, D. C.; Fox, T.; Caldwell, J. W.; Kollman, P. A. A Second Generation Force Field for the Simulation of Proteins, Nucleic Acids, and Organic Molecules. *J. Am. Chem. Soc.* **1995**, *117*, 5179–5197.

(27) Maseras, F.; Morokuma, K. IMOMM: A New Integrated Ab Initio + Molecular Mechanics Geometry Optimization Scheme of Equilibrium Structures and Transition States. *J. Comput. Chem.* **1995**, *16*, 1170–1179.

(28) Svensson, M.; Humbel, S.; Froese, R. D. J.; Matsubara, T.; Sieber, S.; Morokuma, K. ONIOM: A Multilayered Integrated MO + MM Method for Geometry Optimizations and Single Point Energy Predictions. A Test for Diels−Alder Reactions and $Pt(P(t\text{-}Bu)_3)_2 + H_2$ Oxidative Addition. *J. Phys. Chem.* **1996**, *100*, 19357–19363.

(29) Vreven, T.; Morokuma, K. Hybrid Methods: ONIOM(QM:MM) and QM/MM. In *Annual Reports in Computational Chemistry*; Spellmeyer, D. C., Ed.; Elsevier: Amsterdam, The Netherlands, 2006; Vol. 2, Chapter 3.

(30) Vreven, T.; Byun, K. S.; Komáromi, I.; Dapprich, S.; Montgomery, J. A., Jr.; Morokuma, K.; Frisch, M. J. Combining Quantum Mechanics Methods with Molecular Mechanics Methods in ONIOM. *J. Chem. Theory Comput.* **2006**, *2*, 815–826.

(31) Hermann, J. C.; Ridder, L.; Mulholland, A. J.; Holtje, H. D. Identification of Glu166 as the General Base in the Acylation Reaction of Class A β-Lactamases through QM/MM Modeling. *J. Am. Chem. Soc.* **2003**, *125*, 9590–9591.

(32) Hermann, J. C.; Hensen, C.; Ridder, L.; Mulholland, A. J.; Holtje, H. D. Mechanisms of Antibiotic Resistance: QM/MM Modeling of the Acylation Reaction of a Class A β-Lactamase with Benzylpenicillin. *J. Am. Chem. Soc.* **2005**, *127*, 4454–4465.

(33) Hermann, J. C.; Ridder, L.; Hotje, H. D.; Mulholland, A. J. Molecular Mechanisms of Antibiotic Resistance: QM/MM Modelling of Deacylation in a Class A β-Lactamase. *Org. Biomol. Chem.* **2006**, *4*, 206–210.

(34) Hermann, J. C.; Pradon, J.; Harvey, J. N.; Mulholland, A. J. High Level QM/MM Modeling of the Formation of the Tetrahedral Intermediate in the Acylation of Wild Type and K73A Mutant TEM-1 Class A β-Lactamase. *J. Phys. Chem. A* **2009**, *113*, 11984–11994.

(35) Meroueh, S. O.; Fisher, J. F.; Schlegel, H. B.; Mobashery, S. Ab Initio QM/MM Study of Class A β-Lactamase Acylation: Dual Participation of Glu166 and Lys73 in a Concerted Base Promotion of Ser70. *J. Am. Chem. Soc.* **2005**, *127*, 15397–15407.